ISTITUTO NAZIONALE DI FISICA NUCLEARE - ISTITUTO NAZIONALE DI FISICA NUCLEARE - ISTITUTO NAZIONALE DI FISICA NUCLEARE - ISTITUTO NAZIONALE DI FISICA NUCLEARE - ISTITUTO NAZIONALE DI FISICA NUCLEARE - ISTITUTO NAZIONALE DI FISICA NUCLEARE - ISTITUTO NAZIONALE DI

Laboratori Nazionali di Frascati

Submitted to Nucl. Instr. & Meth. in Phys. Res.

LNF-93/030 (P)
21 Giugno 1993

G. Alexander, F. Anulli, D. Babusci, R. Baldini-Ferroli, M. Bassetti, S. Bellucci, I. Cohen, A. Courau, G. Giordano, G. Matone, A. Moalem, M.A. Moinester, G. Pancheri, M. Preger, L. Razdolkaja, P. Sergio, P. Tini-Brunozzi, A. Zallo:

TWO-PHOTON PHYSICS CAPABILITIES OF KLOE AT DAΦNE

PACS.: 13.60.Le; 29.90.+r

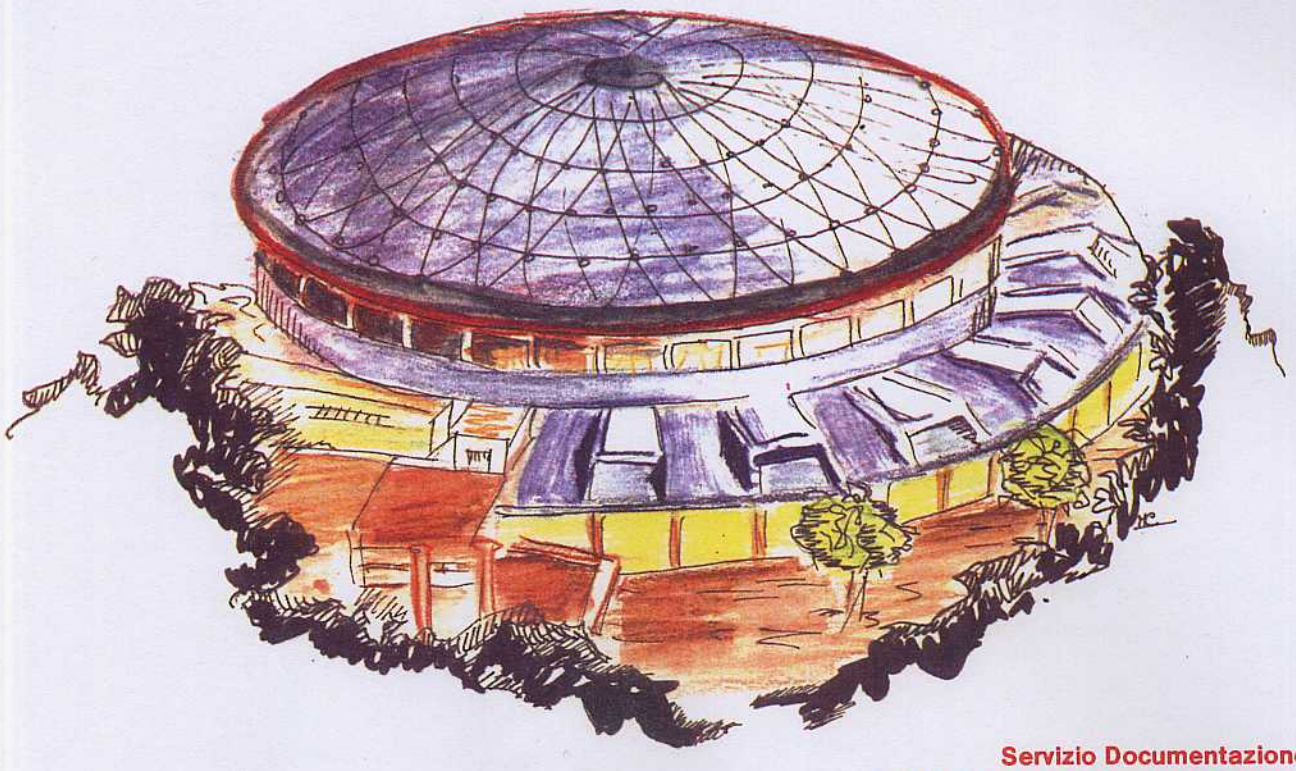

Servizio Documentazione
dei Laboratori Nazionali di Frascati
P.O. Box, 13 - 00044 Frascati (Italy)

INFN - Laboratori Nazionali di Frascati
Servizio Documentazione

LNF-93/030 (P)
21 Giugno 1993

TWO-PHOTON PHYSICS CAPABILITIES OF KLOE AT DAΦNE

G. Alexander[1], F. Anulli[2], D. Babusci[2], R. Baldini-Ferroli[2], M. Bassetti[2], S. Bellucci[2], I. Cohen[1], A. Courau[3], G. Giordano[2], G. Matone[2], A. Moalem[4], M.A. Moinester[1], G. Pancheri[2], M. Preger[2], L. Razdolkaja[4], P. Sergio[2], P. Tini-Brunozzi[5] and A. Zallo[2]

1) School of Physics and Astronomy, Tel-Aviv University, Raymond and Beverly Sackler Faculty of Exact Sciences, 69978 Tel-Aviv, Israel
2) Laboratori Nazionali di Frascati dell' I.N.F.N., I-00044 Frascati, Italy
3) Laboratoire de l'Accelerateur Lineaire, CNRS-IN2P3-Universite de Paris-Sud, 91405 Orsay, France
4) Department of Physics, Ben-Gurion University, 84105 Beer-Sheva, Israel
5) Dipartimento di Fisica dell'Universita' di Perugia and I.N.F.N., Sezione di Perugia, I-06100 Perugia, Italy

Abstract

A feasibility study has been carried out for high precision measurements of two-photon reactions leading to hadrons at the DAΦNE electron-positron collider. This new facility will operate at a CM energy of 1.02 GeV and up to a maximum of 1.5 GeV. It will have a luminosity of $L \simeq 5 \times 10^{32}$ cm^{-2} s^{-1}, 100 times larger than the present available e^+e^- colliders. DAΦNE offers an excellent opportunity to study $\gamma\gamma$ reactions at low energy with high statistics, using the KLOE detector equipped with electron tagging facilities as described in this report. Among the various topics that one may address in these studies, we concentrate on the following: (1) Precision measurements of the polarizabilities of charged and neutral pions via the two-photon reactions $\gamma\gamma \to \pi\pi$. These will allow tests of chiral theories and chiral perturbation techniques, as well as other theoretical approaches. (2) Measurements for the first time of the azimuthal correlations of the $\gamma\gamma \to \pi\pi$ and other two-photon reactions. This provides new tests of the validity of chiral and other theories. (3) Formation of the $C = +1$ light pseudoscalar mesons, π^0, η and η'. This allows the study of the $q\bar{q}$ and possibly gg inner structure of these mesons. For the π^0 its measured radiative width will also improve the currently known life-time. (4) The possibility to realize a double tagging at DAΦNE will allow reliable measurements of the total $\gamma\gamma \to$ *hadrons* cross section below 1 GeV, which currently is vaguely known to be compared with several models. The physics program described above *cannot* be realized without tagging the two-photon reactions to suppress the background from e^+e^- annihilation channels and other sources.

1 Introduction

The subject of photon-photon reactions leading to hadrons and leptons was studied over the last two decades in e^+e^- colliders operated at CM energies of about 10 GeV or more. In general there are two clear deficiencies in the existing measurements. The first is the large statistical and systematic uncertainties, related to the relatively small data samples and background contributions. The second is the very small detection efficiency and particle identification ambiguities for low mass ($\leq$ 500 MeV) hadronic systems. These deficiencies should be absent at DAΦNE [1] when equipped with a large multi-particle detector as KLOE [1]. Due to a combination of high luminosity and favorable kinematical conditions [2], DAΦNE offers the opportunity for new precision measurements of low mass hadronic systems with high statistics and considerably smaller systematic errors.

This can be visualized looking at the luminosity function given in Fig. 1 showing the processes that can be studied now ($\gamma\gamma \to \pi^0\pi^0$, $\gamma\gamma \to \pi^+\pi^-$, π^0 and η production) and the processes that will require an energy upgrade of the machine (η' and f_0 production). Integrating this function, under the assumption of full acceptance of the detector, one year of data taking (10^7 s) and a machine luminosity of $L \simeq 5 \times 10^{32}$ cm^{-2} s^{-1}, one yields the following rates (for more details see [4, 5]):

a) $\simeq 10^4$ events/year for $\gamma\gamma \to \pi^0\pi^0$

b) $\simeq 10^6$ events/year for $\gamma\gamma \to \pi^+\pi^-$

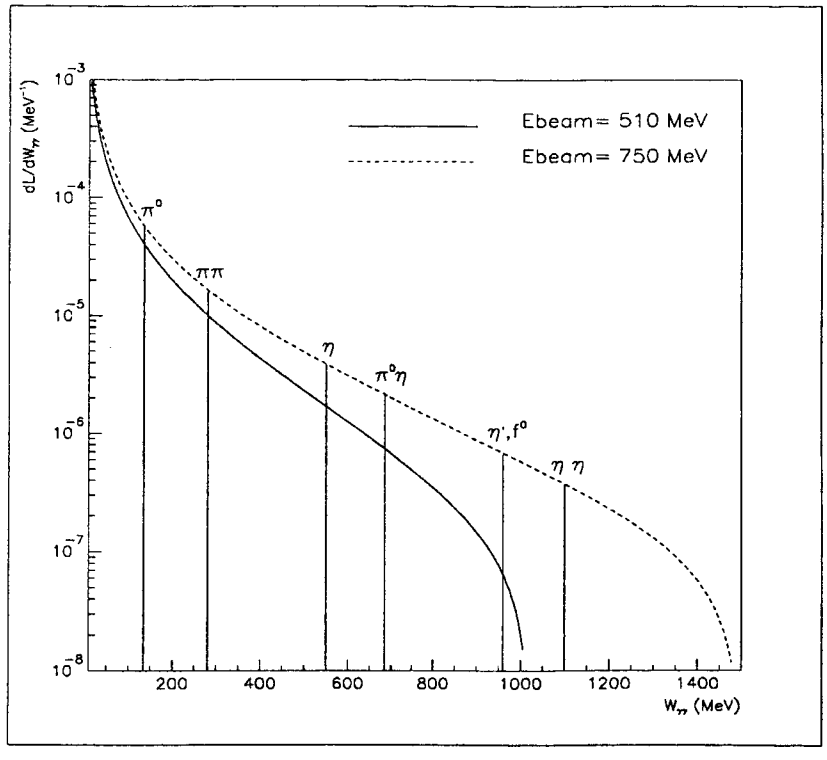

Figure 1: Photon-photon flux at DAΦNE as function of $W_{\gamma\gamma}$

There are many physics questions that one may address in two-photon studies at DAΦNE. Among these four are pertinent to this study, namely:

(1) Production of charged and neutral meson-antimeson pairs. This probes different theories from which one can measure the polarizability of these mesons.
(2) Measurements of the azimuthal correlations which so far could not be performed at the

existing colliders. This constitutes a unique contribution to DAΦNE.
(3) Coupling of neutral $C = +1$ mesons to a photon-pair through the reaction $\gamma\gamma \rightarrow$ *neutral meson*. This coupling depends on the inner structure of the meson and its quark-antiquark (and possibly gluon-antigluon) structure.
(4) Total $\gamma\gamma \rightarrow$ *hadrons* cross section below 1 GeV.

In order to isolate experimentally these processes and suppress systematic errors arising from non-$\gamma\gamma$ interactions, it is necessary to detect at least one of the scattered electrons (single tag mode). With DAΦNE this can be done more easily than with machines that work with more high energy. In fact for PEP/PETRA the electrons are produced at an average scattering angle $\theta \simeq m/E \simeq 10^{-2}$ mrad, while for DAΦNE this angle is $\theta \simeq 1$ mrad (Fig. 2).

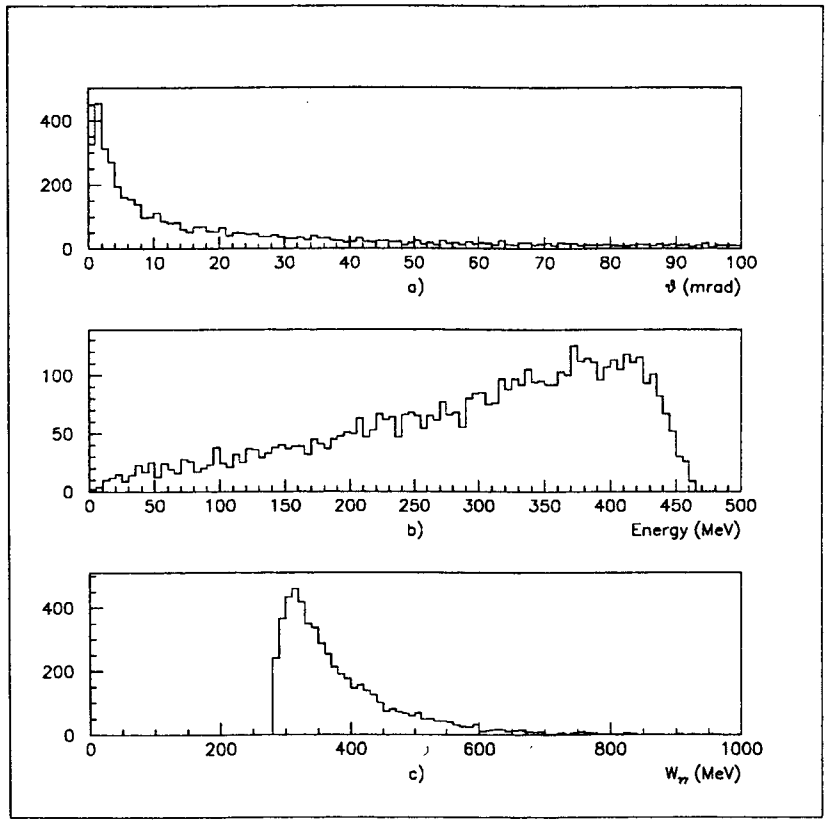

Figure 2: $e^+e^- \rightarrow e^+e^-\pi\pi$. a) electron scattering angle; b) electron energy; c) $\gamma\gamma \rightarrow \pi^0\pi^0$ invariant mass.

This advantage can be exploited only partially owing to the limits imposed by the low β insertion quadrupoles and by the minimum angle covered by the central detector.

Also shown in Fig. 2 is the energy of the scattered electrons and the produced mass distribution ($e^+e^- \rightarrow e^+e^-\pi\pi$). In particular the mass distribution shows the possibility to study with high luminosity the region below 500 MeV.

It should be noted that the requirement of tagging reduces the statistics of the data sample. We have investigated and found it possible to equip DAΦNE with an electron tagging facility in conjunction with its detector KLOE. In fact, because of the rather high

luminosity, one can accumulate high enough statistics even in the double tag mode. This should eliminate the contributions from competing background processes and should allow precision measurements to be made.

The report is organized as follows. In Section 2 we present the physics interest in studying two-photon reactions at DAΦNE. Section 3 is devoted to our study of the tagging and to the feasibility of realizing such a facility at DAΦNE-KLOE. The absolute cross sections measurements do depend also on the luminosity determination, which is briefly discussed in Section 4. A summary and conclusions are given in Section 5.

2 Physics Topics

Polarizabilities of Pions

The electric ($\bar{\alpha}$) and magnetic ($\bar{\beta}$) polarizabilities [6] of any composite system are fundamental quantities introduced to take into account phenomenologically the influence of the internal structure of the system on their two-photon interactions at low energy.
The experimental determination of these quantities constitutes an important testing ground for any hadron model and can be obtained from precise measurements of the $\gamma h \to \gamma h$ Compton scattering or $\gamma\gamma \to h\bar{h}$ differential cross sections. In recent years, a great deal of interest has been expressed in the literature for the polarizabilities of the pion [7, 8, 9, 10, 11, 12, 13] which belongs to the pseudoscalar meson nonet and thus is believed to be one of the Goldstone bosons associated with the spontaneously broken chiral symmetry.

Chiral perturbation theory (χPT) [14] is expected to successfully describe the electromagnetic interactions of pions [15, 16, 17, 18, 19]. In this framework, the low energy interactions of the Goldstone bosons are described by an effective Lagrangian which stems directly from QCD, with only the assumptions of chiral symmetry $SU(3)_L \otimes SU(3)_R$, Lorentz invariance and low momentum transfer. In particular, with a perturbative expansions of this Lagrangian limited to terms of increasing order in the external momenta and quark masses, the theory is capable of establishing a network of relationships between different processes in terms of a common set of renormalized parameters L_i^r (tree level coefficients). At $O(p^4)$-level, the perturbative expansion is truncated at terms quartic in the photon momentum and 12-coupling constants are needed. For example, in the charged case, the radiative pion beta decay and electric polarizability are expressed as [17]:

$$h_A/h_V = 32\pi^2(L_9^r + L_{10}^r)\,, \qquad \bar{\alpha}_\pi = \frac{4\alpha}{m_\pi F_\pi^2}(L_9^r + L_{10}^r) = -\bar{\beta}_\pi\,, \tag{1}$$

where $F_\pi = (93.15 \pm 0.11)$ MeV is the pion decay constant [20] and α is the fine structure constant. The pion beta decay determination $h_A/h_V = 0.45 \pm 0.07$ [21] leads to $L_9^r + L_{10}^r$ $= (1.42 \pm 0.22) \times 10^{-3}$ and then the χPT prediction is [1]

$$\bar{\alpha}_{\pi^\pm} = 2.68 \pm 0.42\,. \tag{2}$$

For the neutral pion polarizability the situation is different. Since only neutral particles are involved in this case, the Born term vanishes and therefore, at the lowest $O(p^4)$-level, the $\gamma\gamma \to \pi^0\pi^0$ cross section can only be generated by a finite 1-loop diagram and hence provides a unique testing ground for the loop structure of χPT. The polarizability is a parameter-free prediction given by the following expression [7]

$$\bar{\alpha}_{\pi^0} = -\bar{\beta}_{\pi^0} = -\frac{\alpha}{96\pi^2 m_\pi F_\pi^2} = -0.498 \pm 0.001\,. \tag{3}$$

The experimental knowledge that is presently available on the pion polarizabilities has been reviewed in Ref. [13].

[1] In the present paper the polarizabilities are expressed in Gaussian units of 10^{-43} cm^3.

Table 1: Charged Pion Electrical Polarizability $\bar{\alpha}$ in units of 10^{-43} cm^3

Experiment	$\bar{\alpha}$
$\gamma\gamma \to \pi^+\pi^-$ PLUTO [24]	$19.1 \pm 4.8(stat.) \pm 5.7(syst.)$
$\gamma\gamma \to \pi^+\pi^-$ DM1 [25]	$17.2 \pm 4.6(stat.)$
$\gamma\gamma \to \pi^+\pi^-$ DM2 [26]	$26.3 \pm 7.4(stat.)$
$\gamma\gamma \to \pi^+\pi^-$ MARKII [22]	$2.2 \pm 1.6(stat. + syst.)$
$\pi Z \to \pi Z\gamma$ Serphukov [23]	$6.8 \pm 1.4(stat.) \pm 1.2(syst.)$
$\gamma Z \to \pi Z\gamma$ Lebedev [27]	$20. \pm 12.(stat.)$
Theory (χPT)	2.7 ± 0.4

Table 1 summarizes the results which have been obtained considering all the data available for the charged pion both in the Compton and photon-photon channels. The wide range of values is a clear indication of the large systematic uncertainties that affect all these experimental determinations. The most significant values come from the MARK-II [22] and Serphukov [23] experiments. The former is consistent with the chiral prediction (see Fig. 3) but the latter differ by more than two standard deviations from the value of Eq.(2). Other experimental determinations have been obtained in Ref. [13], using the data published by PLUTO [24], DM1 [25], DM2 [26], and Lebedev [27] groups.

As for the π^0, the only source of information comes from the Crystal Ball data on the $\gamma\gamma \to \pi^0\pi^0$ reaction (see Fig. 4). In the χPT 1-loop approximation discussed in Ref. [13], this data set determines an experimental value for the absolute value of π^0 polarizability of:

$$| \bar{\alpha}_{\pi^0} | = 0.69 \pm 0.07(stat.) \pm 0.04(syst.) \qquad (4)$$

This result is 40% larger than the chiral prediction of Eq.(3). This discrepancy could be reduced within χPT by including also higher order contributions. However, the $O(p^6)$ contribution due to the vector-meson exchange in the t-channel [4, 9, 18] does not cure this discrepancy. In fact the dispersive approach [29], a recent 2-loop calculation [30] (see Fig. 4) and a recent mixed chiral-dispersive approach [31] all indicate better agreement with the data.

A quantitative analysis of the standard approximation of considering only real photons for the detection of the $\gamma\gamma \to \pi^0\pi^0$ signal has been given recently [32]. This shows that a measurament of the azimuthal correlations would test the higher order χPT corrections indipendently from the cross section measurament. The authors of [32] approximate these corrections by including the contributions in the scattering amplitude.

The available mass range at DAΦNE for the study of these processes is from threshold to $\simeq 0.6$ GeV. Therefore one will have the possibility to improve significantly the statistical and systematical errors of the polarizability measurements. For a luminosity of $L \simeq 5 \times 10^{32}$ cm^{-2} s^{-1} one should expect $\simeq 1.0 \times 10^4$ events/year, for the $\gamma\gamma \to \pi^0\pi^0$ reaction. This will give a statistical error [33] at the level of 5% in a 10 MeV mass bin from threshold to 500 MeV. For the process $\gamma\gamma \to \pi^+\pi^-$, we expect 1.8×10^6 events/year. This cross-section is dominated by the Born amplitude and the contribution of the charged pion polarizability is small (the Born contribution at *e. g.*, $\sqrt{s} = 0.4$ GeV is 90% of the total cross section). Owing to this, the χPT corrections will be measured with no better accuracy than the $\pi^0\pi^0$ case.

Choosing the value of $(L_9^r + L_{10}^r)$ as obtained from one experimental point, namely at $\sqrt{s} = 0.4$ GeV, in order to have a 5% statistical accuracy on this measurement of $(L_9^r + L_{10}^r)$, one needs a 0.6% statistical error on the measured cross section [33]. So if we have 25 bins in energy it will require a statistical error of 3% in each bin.

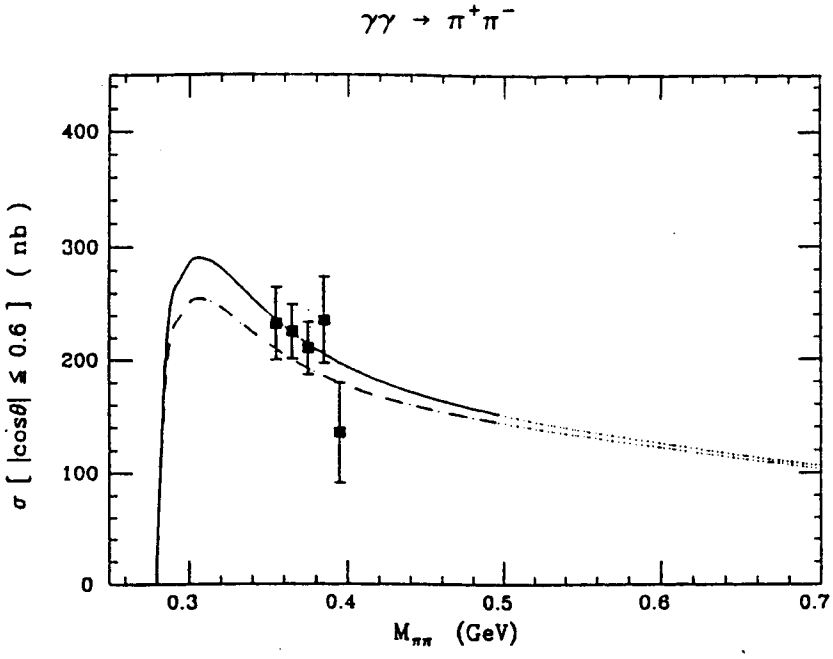

Figure 3: MARK-II total cross-section data for $M_{\pi\pi} \leq 0.5$ GeV. The theoretical curves are: Born (dash-dot line); χPT with $(L_9^r + L_{10}^r) = 1.4 \times 10^{-3}$ (full line). The region above $M_{\pi\pi} = 0.5$ GeV is considered to be outside the domain of validity of χPT.

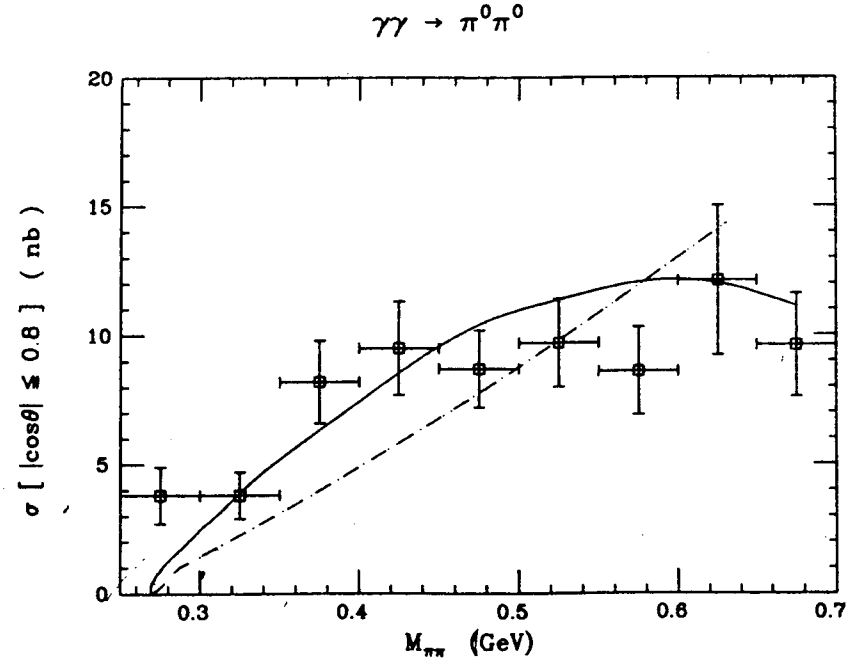

Figure 4: The cross-section for $\gamma\gamma \to \pi^0\pi^0$: i) the 1-loop contribution (dash-dot line); ii) the 2-loop contribution (full line). The data are taken from the Crystal Ball experiment.

Azimuthal Correlation Measurements

At DAΦNE, one can study the production of hadrons close to threshold with "quasi-real" photon collisions via the $e^-e^+ \to e^-e^+ hadron(s)$ reaction. Unlike the case at higher energy colliders, the study of this reaction at DAΦNE involves wide angular distributions of the final state electrons [2]. For example we estimate that 50% of the electrons are scattered at angles $\theta > 10$ mrad, while 16% have $\theta > 100$ mrad.

Of particular interest are the azimuthal (ϕ) correlations that can be measured for two-photon reactions [34, 35, 36]. Here we consider the $\gamma\gamma' \to \pi^+\pi^-$ and $\gamma\gamma' \to \pi^0\pi^0$ processes, corresponding to $e^-e^+ \to e^-e^+\pi\pi$ reactions. The ϕ dependence is most easily given by writing the cross section in terms of helicity amplitudes $B_{m\bar{m},n\bar{n}}$, where $m\bar{m}$ and $n\bar{n}$ stand respectively for the helicity values of the γ (associated with e^-) and γ' (associated with e^+). The unbarred and barred indices correspond to the matrix element and its conjugate. For "quasi-real" photons, one has the helicity values for transverse photons $m, \bar{m}, n, \bar{n} = +1$ and -1 only. Neglecting longitudinal photons (helicity zero), there remain six $B_{m\bar{m},n\bar{n}}$ helicity amplitudes (instead of twenty) which are: $B_{++,++}$, $B_{++,--}$, $B_{++,+-}$, $B_{+-,++}$, $B_{+-,+-}$, $B_{+-,-+}$. For the differential cross section, one obtains:

$$d\sigma/d\Omega \propto A_0 - 2A_1(\epsilon \cos 2\phi_1 + \epsilon' \cos 2\phi_2) + \epsilon\epsilon'(A_3 \cos 2\phi_3 + A_4 \cos 2\phi_4) \,, \tag{5}$$

where $\phi_3 = \phi_1 + \phi_2$ and $\phi_4 = \phi_1 - \phi_2$, and the A_i in the $\gamma\gamma'$ CM are in general functions of the polar angle θ_i. The angles ϕ_1, ϕ_2 shown in Fig. 5 are azimuthal angles in the $\gamma\gamma'$ CM frame between one of the pions produced (either one) and the two outgoing electrons. Experimentally, $\cos(2\phi)$ is found from the angle measurements with respect to either one of the two pions. In terms of the helicity amplitudes, we have:

$$\begin{aligned} A_0 &= B_{++,++} + B_{++,--} \,, \quad & A_3 &= B_{+-,+-} \,, \\ A_1 &= B_{++,+-} = B_{+-,++} \,, \quad & A_4 &= B_{+-,-+} \,. \end{aligned} \tag{6}$$

The polarization parameters of the photons ϵ and ϵ' are given in terms of E_γ and $E_{\gamma'}$, respectively and of the incident beam energy E. For ϵ, for example, the expression is:

$$\epsilon = [1 - E_\gamma/E]/[1 - (E_\gamma/E) + (E_\gamma/E)^2/2] \,. \tag{7}$$

The various expressions for A_i depend now on the model. If the Born term is taken for $\gamma\gamma' \to \pi^+\pi^-$, then $A_i = f_i(u, \beta)$ are functions of u and β, the cosine of the emission angle and the velocity of the π^+ in the $\pi^+\pi^-$ rest system, respectively:

$$\begin{aligned} A_0 &= \frac{(1-\beta^2)^2 + \beta^4(1-u^2)^2}{(1-\beta^2u^2)^2} \,, \quad & A_3 &= \frac{(1-\beta^2)^2}{(1-\beta^2u^2)^2} \,, \\ A_1 &= \frac{\beta^2(1-\beta^2)(1-u^2)}{(1-\beta^2u^2)^2} \,, \quad & A_4 &= \frac{\beta^4(1-u^2)^2}{(1-\beta^2u^2)^2} \,. \end{aligned} \tag{8}$$

Note that, the azimuthal ϕ_i angles are defined in a perpendicular plane of the $\gamma\gamma'$ CM system which moves with respect to the laboratory system and cannot always be determined. However, this $\gamma\gamma'$ CM always moves very close to the e^+e^- beam axis which is well defined. For this reason we present in the following the azimuthal angular distributions in a plane perpendicular to the e^+e^- beam axis.

The azimuthal correlations as observed in the e^+e^- system are given in Fig. 6.

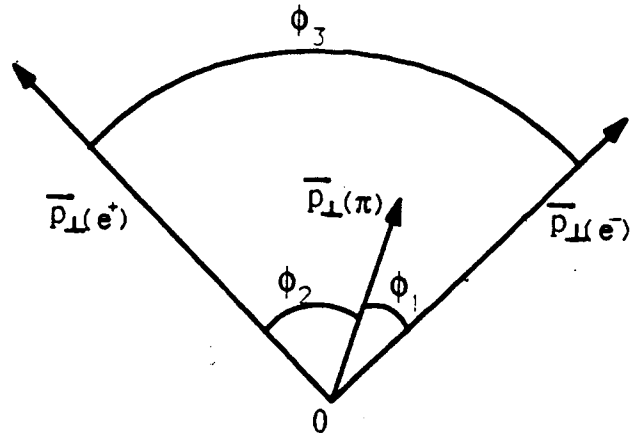

Figure 5: Kinematics defining the azimuthal angles. $\vec{p}_{perp}(e^-)$, $\vec{p}_{perp}(e^+)$, $\vec{p}_{perp}(\pi)$, are the projections of $\vec{p}(e^-)$, $\vec{p}(e^+)$, $\vec{p}(\pi)$ onto the plane transverse to the $\gamma\gamma$ collision axis. Also, $\phi_3 = \phi_1 + \phi_2$ and $\phi_4 = \phi_1 - \phi_2$.

In this figure the polar angle range for the detected pions is set by the KLOE acceptance. A complete calculation for the $\pi^+\pi^-$ case must include the pion polarizability contributions which will however only make small changes in the correlations.

In the case of $\gamma\gamma \to \pi^0\pi^0$, up to O($p^4$), the A_i are θ-independent [15, 16, 19, 35, 36] and we obtain in the $\gamma\gamma'$ CM system:

$$A_0 = A_3 = |A^{ch}|^2 \frac{W_{\gamma\gamma}^4}{4} \,, \qquad A_1 = A_4 = 0 \,, \tag{9}$$

where

$$A^{ch} = \frac{\alpha(W_{\gamma\gamma}^2 - m_\pi^2)J}{\pi F_\pi^2 W_{\gamma\gamma}^2} \tag{10}$$

and J is a complex quantity:

$$\Re J = 1 + \frac{m_\pi^2}{W_{\gamma\gamma}^2}[\ln^2 \frac{z_+}{z_-} - \pi^2] \tag{11}$$

$$\Im J = -2\pi \frac{m_\pi^2}{W_{\gamma\gamma}^2} \ln \frac{z_+}{z_-} \tag{12}$$

with

$$z_\pm = \frac{1}{2}\left[1 \pm \sqrt{1 - \frac{4m_\pi^2}{W_{\gamma\gamma}^2}}\right] \tag{13}$$

The corresponding correlations for this case are shown in Fig. 7.

The angular correlation in ϕ_3 for this model (A_3 determination) has a more interesting azimuthal dependence whose magnitude is related to the polarizability value. The azimuthal correlations in this χPT calculation do not change when vector meson dominance contributions are added [4, 18, 32]. The agreement of these ϕ correlations with these expectations

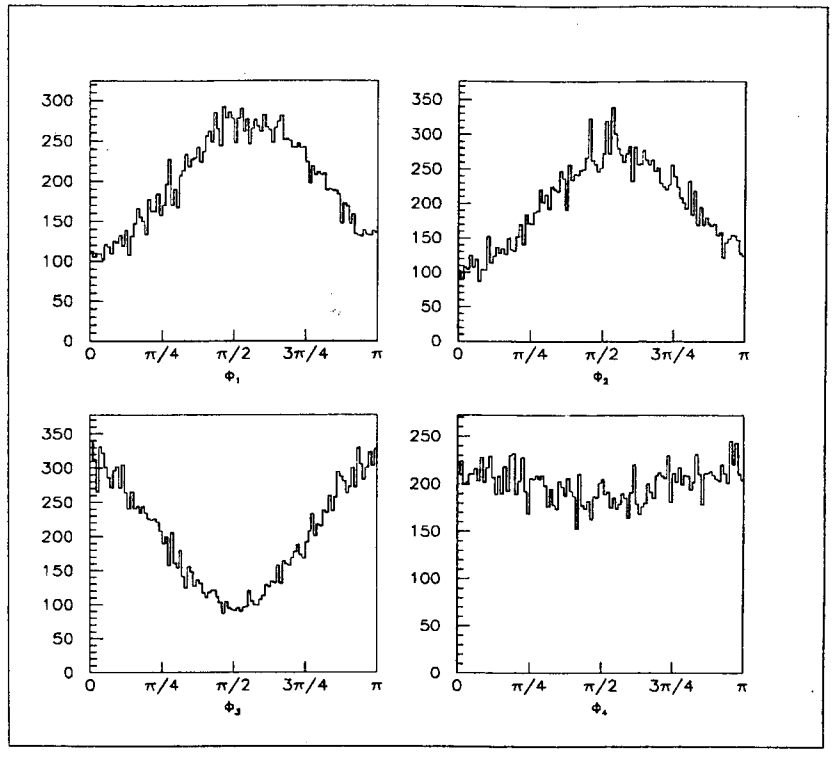

Figure 6: The azimuthal correlation in the e^+e^- system for the Born term.

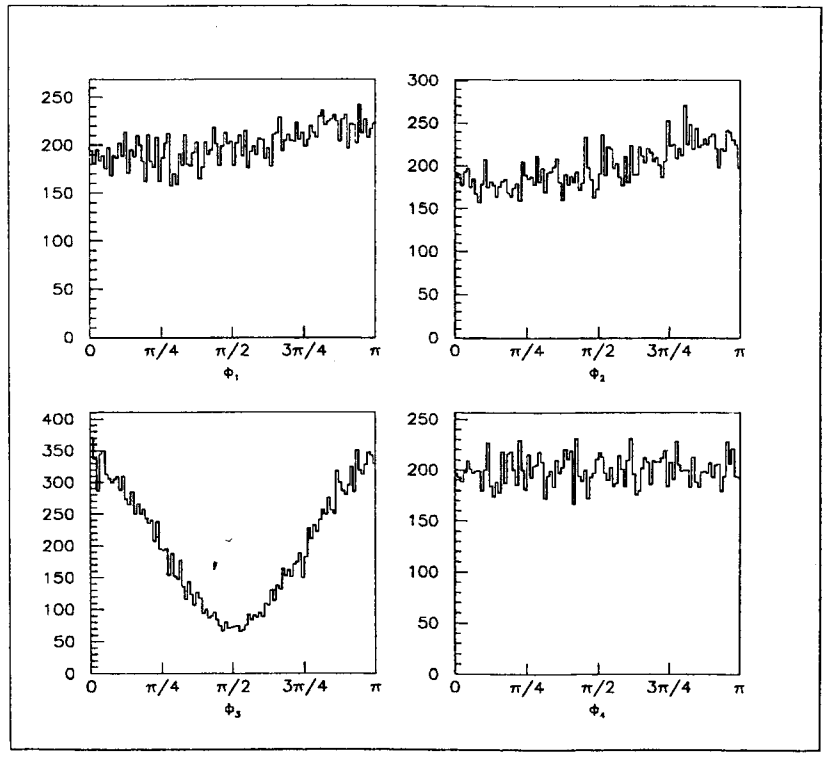

Figure 7: The azimuthal correlation in the e^+e^- system for Chiral Models.

Table 2: Radiative Decay Width for Light Pseudoscalar Mesons.

Meson	Mass (MeV)	$\Gamma_{\gamma\gamma}$(eV)	Experiment	Comment
π^0	134.9743 ± 0.0008	7.8 ± 0.5		*Average Value*
		11.6 ± 1.24	*CNTR*	*Primakoff*
		7.22 ± 0.55	*CNTR*	*Primakoff*
η	547.45 ± 0.19	460 ± 40		*Average Value*
		$530 \pm 40 \pm 40$	*JADE*	$e^-e^+ \rightarrow e^-e^+P$
		324 ± 46	*CNTR*	*Primakoff*
η'	957.75 ± 0.14	4290 ± 190		*Average Value*
		$3620 \pm 140 \pm 480$	*CELLO*	$e^-e^+ \rightarrow e^-e^+P$
		$4940 \pm 230 \pm 720$	*ASP*	$e^-e^+ \rightarrow e^-e^+\gamma\gamma$

determines to what extent these chiral predictions are correct and consequently also the reliability of polarizability determinations that use chiral formulae.

Non-chiral based models are available for the π^0 polarizability and can be compared to the experimentally determined azimuthal correlations, if the associated azimuthal predictions become available. The correlations can be measured for different polar angle regions and for different regions of $W_{\gamma\gamma}$. The correlation data will also allow extra consistency checks on the data for helping define the systematic uncertainties in the measurements for tagged events. This measurements can be carried out not only in the double-tag but also in the single-tag mode. In the former all the correlation angles are accessible. In the single-tag mode only one angle (ϕ_1 or ϕ_2) can be measured. Nevertheless the distribution of this angle is significantly different between the Born case and chiral case as is evident from the Figs. 6 and 7.

Radiative Width $\Gamma_{\gamma\gamma}$ of Light Mesons

Meson formation via $\gamma\gamma$ reactions at e^-e^+ colliders have been studied in the past in no-tag experiments [37]. However, these experiments yielded radiative decay width values of limited accuracy. In Table 2 are listed the results for the π^0, η and η' radiative decays, taken from the latest edition of the Particle Data Group [20], where the minimum, maximum, and averaged measured values are shown. Note that for the π^0 we list the decay width values, rather than the life-time given in Ref. [20]. The combination of the high Luminosity of the DAΦNE machine and the superb characteristics of the KLOE detector [1] offers an excellent opportunity for precision measurements of the radiative decay widths (decay constants) via meson formation in $\gamma\gamma$ collisions.

The radiative decay widths, $\Gamma^{PS}_{\gamma\gamma}$, of the Pseudoscalar mesons (PS) constitute fundamental characteristics of the inner structure of the mesons and their strong interactions. Using the triangle diagram and assuming partial conservation of the axial current (PCAC), the radiative width can be written as

$$\Gamma^{PS}_{\gamma\gamma} = \frac{\alpha^2}{32\pi^3}\frac{M^3_{PS}}{f^2_{PS}}[\Sigma_{color} < e^2_q >]^2, \qquad (14)$$

where M_{PS} is the meson mass and f_{PS} is the meson decay constant. In this last equation the $< e^2_q >$ represents the average of the square of the quark charges, referred to as the charge form factor. In the nonet hypothesis, the decay constant can assume an octet $f_{PS} =$ f_8 or a singlet $f_{PS} = f_1$ value, and the charge form factors are $1/(3\sqrt{2})$, $1/(3\sqrt{6})$ and $2/(3\sqrt{3})$ for the π^0, the η_8 and the η_1 respectively.

Table 3: $(e^-e^+ \to e^-e^+PS)$ events/year

Meson[1]	Total Production Rate	Single-Tag Events	Double-Tag Events
π^0	2.0×10^6	5.0×10^5	2.0×10^4
η	5.0×10^5	7.5×10^4	2.5×10^3
η'	1.0×10^5	5.7×10^4	1.4×10^3

1) The values for π^0 and η are for an incident beam energy $E = 510$ MeV. The value for the η' is for $E = 750$ MeV.

The interest in the coupling of π^0 to $\gamma\gamma$ is obvious as it constitutes a direct measurement of the π^0 life-time. The best value so far given for the width of π^0 to $\gamma\gamma$ is that of the Crystal Ball detector at DORIS II [38]:

$$\Gamma(\pi^0 \to \gamma\gamma) = 7.7 \pm 0.5 \pm 0.5 \text{ eV} . \tag{15}$$

We expect to improve this measurement considerably by using tagged events. Precise measurement of the η and π^0 radiative width allows for a determination of the pseudoscalar nonet mixing angle θ, through the relation:

$$\frac{\Gamma^{\eta}_{\gamma\gamma}}{\Gamma^{\pi^0}_{\gamma\gamma}} = \frac{1}{3}\left(cos\theta - 2\sqrt{2}sin\theta\right)^2 \left(\frac{m_\eta}{m_{\pi^0}}\right)^3 ,$$

as well as to test the assumption $f_8 = f_1$, through the relation:

$$R = \left[\frac{\Gamma^{\eta}_{\gamma\gamma}}{m^3_\eta} + \frac{\Gamma^{\eta'}_{\gamma\gamma}}{m^3_{\eta'}}\right] \frac{m^3_{\pi^0}}{\Gamma^{\pi^0}_{\gamma\gamma}} = (1 + 8r^2)/3 . \tag{16}$$

where $r = f_1/f_8$. Note that the last expression is independent of the mixing angle which relates the physical η and η' to η_1 and η_8, and that $R = 3$ for $f_8 = f_1$ [39].

We next estimate the expected rates and width precisions expected from the proposed two-photon experiment at DAΦNE. Using the relativistic Breit-Wigner formula for the $\gamma\gamma \to PS$ reaction and the double equivalent photon approximation, the production cross section can be written in the form:

$$\sigma_{ee\to eePS} = 64\alpha^2[ln(E/m)]^2 ln(2E/M_{PS}) \frac{\Gamma^{PS}_{\gamma\gamma}}{M^3_{PS}} , \tag{17}$$

where E and m are the beam energy and the electron mass. To estimate the production rate/year we take the luminosity to be $L \simeq 5 \times 10^{32}$ cm^{-2} s^{-1} and integrate over a year of 10^7 s. The results are listed in Table 3. In column 3 and 4 we include the expectations for single and double-tag event rates, taking into account the KLOE acceptance for π^0 or η decay to $\gamma\gamma$ and the tagging acceptances discussed in Sec. 3. As seen from the Table, the π^0 and η mesons will be produced abundantly in DAΦNE and the data should yield radiative widths with statistical errors better than 1%.

DAΦNE is expected at a later phase to operate at higher energies up to about 1.5 GeV of total CM energy. This would allow measurements of the radiative widths of higher mass pseudoscalars like the η' itself as well as that of the elusive scalar mesons, such as the $f_0(975)$ whose structure is still unclear.

Judging from the values quoted in Table 2, the experimental situation is far from being satisfactory. Using the average mass and the average decay width values given in Table 2, one calculates the ratio R to be:

$$R \pm \Delta R = 2.5 \pm 0.4(stat) \pm 0.4(syst) . \tag{18}$$

Due to the large errors, the measured R is consistent with the value 3 within one standard deviation. This situation calls for more precise measurements of the radiative decay widths.

$\gamma\gamma$ Total Hadronic Cross Section

The values of the total $\gamma\gamma$ hadronic cross section around and below 1.5 GeV are not measured or are only very poorly known and also differ from experiment to experiment. The main reason for this situation comes from the fact that in no-tag and single-tag experiments, one is unable to determine the $W_{\gamma\gamma}$ value event by event. For this reason, unfolding procedures were used to deduce $W_{\gamma\gamma}^{obs}$ from the observed CM energy distribution [41]. These procedures, however, were found to be unreliable and often not reproducible, a fact that may account for the various non-compatible experimental results (PLUTO [42], TPC/2γ [43]) at low energies ($\leq$ 2.5 GeV) (see Fig. 8) of the total hadronic $\gamma\gamma$ cross section [44].

There are several attempts to account for the total hadronic $\gamma\gamma$ cross section as well as exclusive cross sections like $\gamma\gamma \to \rho^0\rho^0$ in terms of hadron-hadron and photon-hadron cross sections [45, 46, 47, 48]. These models yield similar results at high $W_{\gamma\gamma}$ values, but differ considerably at the low values accessible to DAΦNE. The KLOE detector equipped with tagging devices presents an excellent opportunity to measure these processes, so far never measured at low energies, using double tag events so that $W_{\gamma\gamma}$ can be evaluated event by event.

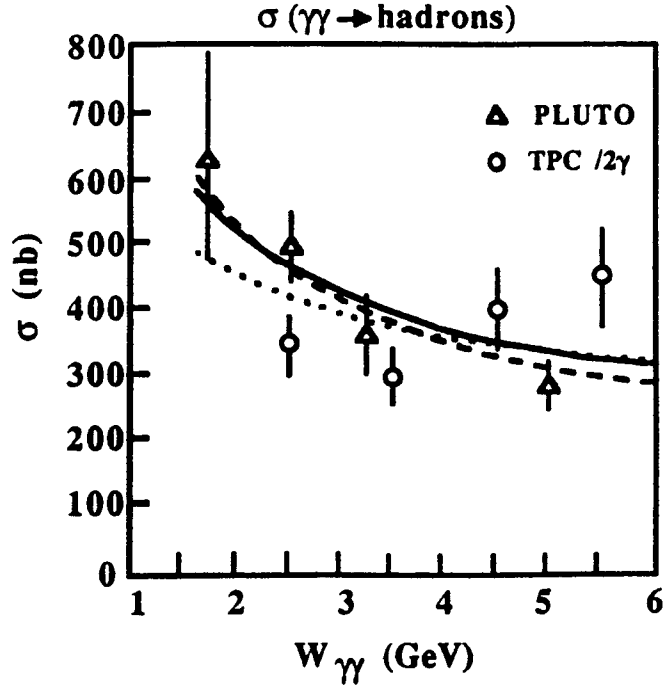

Figure 8: Compilation of the total $\gamma\gamma \to$ *hadrons* cross section as a function of $W_{\gamma\gamma}$ from PLUTO and TPC/2γ experiments. The data are compared with three t-channel factorization models described in Ref. [44].

In addition to the total cross section, the cross section of several exclusive $\gamma\gamma$ reactions can also be studied. For example, the width of the decay process $\eta \to \pi^0\gamma\gamma$ is particularly interesting. The measured value is [20]:

$$\Gamma(\eta \to \pi^0\gamma\gamma) = 0.84 \pm 0.18 \text{ eV} . \tag{19}$$

On the theoretical side, the χPT at $O(p^4)$-level predicts $\Gamma(\eta \to \pi^0\gamma\gamma) \simeq 3.9 \times 10^{-3}$ eV [49, 50]. The authors of Ref. [48] have shown that even including the $O(p^6)$ contributions

coming from the vector (ρ, ω) mesons exchanges in the t and u channels and the scalar [$a_0(980)$] and tensor [$a_2(1310)$] resonances in the s channel, as well as the $O(p^8)$ 1-loop diagrams with two vertices taken from the Wess-Zumino anomaly, this discrepancy cannot be completely cured. They obtain:

$$\Gamma(\eta \to \pi^0\gamma\gamma) = 0.42 \pm 0.20 \text{ eV} . \tag{20}$$

The inclusion of the $O(p^8)$ contribution coming from the C-odd axial-vector resonances [$b_1(1235), h_1(1170), h_1(1380)$] in the t and u channel [51] gives a 10% increase to Eq. (20).

Other interesting channels are $\gamma\gamma \to 3\pi$, $\gamma\gamma \to K^+K^-$, and $\gamma\gamma \to K^0\overline{K}^0$. The last reaction is observed via $\gamma\gamma \to K^0_S K^0_S$ and $\gamma\gamma \to K^0_L K^0_L$.

3 Tagging of $\gamma\gamma$ Events

In the study of tagging at DAΦNE at the $\phi(1020)$-energy we address the following items:

(1) Why tagging is needed for two-photon studies at DAΦNE.
(2) Which is the possibility to equip KLOE with tagging facilities taking into accounts the constraints imposed by the already existing design of the machine lattice and the detector.
(3) What would be the overall acceptance of such facilities for tagged electrons (*i.e.*, final state electrons from two-photon processes).
(4) How well can one eliminate background events with tagging and how would this affect the statistical and systematic errors of the proposed measurements.
(5) Given a tentative design of the tagging detectors, how well can they survive in the high flux from the radiative Bhabha scattering and other sources.
(6) The performance of the tagging facilities in the environment of KLOE.

As was seen in previous $\gamma\gamma$ experiments, the single-tag sample is typically reduced by a factor 5 to 10 compared to the no-tag sample and additional similar reduction occurs for double-tag data. At the same time, the tagged samples are by far less contaminated by background and such events furnish additional information. For physics and background reasons, to be discussed further on, we base our proposal on the study of $\gamma\gamma$ reactions in the double-tag mode. Future experience in running DAΦNE and KLOE will show whether this requirement can be relaxed and to what extent useful results can also be obtained from the single-tag data.

3.1 Why Tagging is Needed ?

The pion polarizability study with the detector KLOE using $\gamma\gamma \to \pi^+\pi^-$ and $\gamma\gamma \to \pi^0\pi^0$ has to be regarded as a second generation experiment after those of SLAC [22] and DESY [28] and their subsequent analysis in term of polarizability. This requires a high statistics and lower systematic errors which cannot be achieved without a strong reduction of background events.

To illustrate how compelling is the tagging, we consider in Table 4 the main sources of e^+e^- annihilation background that can contaminate our $\gamma\gamma \to \pi\pi$ event sample. Based on the values of events/year, the background exceeds by more than three orders of magnitude the expected yield of 1.0×10^4 and 1.8×10^6 for $\gamma\gamma \to \pi^0\pi^0$ and $\gamma\gamma \to \pi^+\pi^-$ respectively (see Sect. 2). Since $\gamma\gamma$ events have essentially zero transverse momentum sum, one can apply a $\sum P_T^2$ balance cut on the hadrons detected by the central detector. Doing this one obtains a rejection factor of $\simeq 30$ [52] but still short of a factor of $\simeq 100$ which must be provided by the tagging facilities. Note that at low e^+e^- energy the two-photon selection criterion E_{vis}/E_{CM} cannot be applied due to the low particle multiplicity. We conclude therefore,

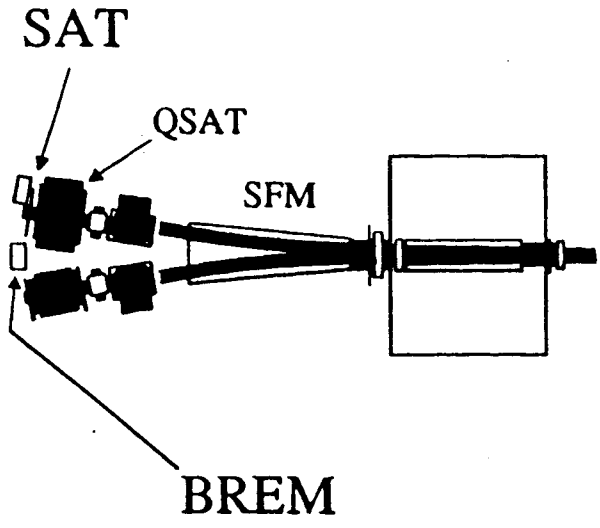

Figure 9a – The small angle tagger SAT, the BREM detector and the modified quadrupole QSAT (top view).

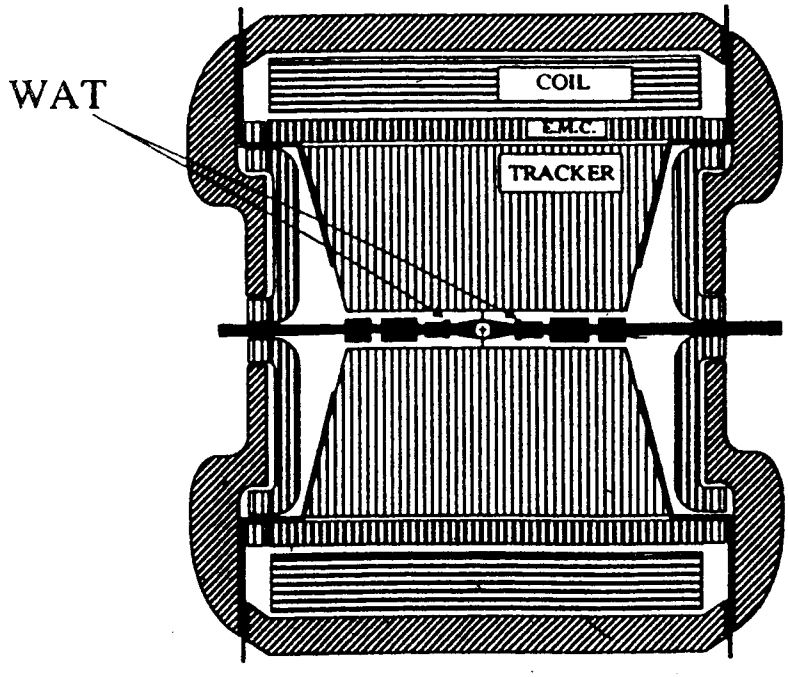

Figure 9b – The wide angle (WAT) tagger insertion in the KLOE detector (side view).

Table 4: Background from Annihilation Events

ϕ Decay Mode[1]	Escaped Particle[3]	Events/Year[2]	$\gamma\gamma$ Process
$K_S^0(\pi^0\pi^0)\ K_L^0$	K_L^0	2.7×10^8	$\pi^0\pi^0$
$\eta(3\pi^0)\ \gamma$	π^0, γ	4.2×10^5	$\pi^0\pi^0$
$K_S^0(\pi^+\pi^-)\ K_L^0$	K_L^0	5.9×10^8	$\pi^+\pi^-$
$\rho(\pi^+\pi^-)\ \pi^0$	π^0	1.3×10^7	$\pi^+\pi^-$
$(\pi^+\pi^-)\ \pi^0$	π^0	2.4×10^6	$\pi^+\pi^-$
$\eta(\pi^+\pi^-\pi^0)\ \gamma$	π^0, γ	3.1×10^5	$\pi^+\pi^-$

1) The particles in parentheses are assumed to be detected in KLOE.
2) Events/year corresponds to 10^{10} $\phi(1020)$ produced per year.
3) The escape probability of the γ not included.

that the polarizability measurements at DAΦNE cannot be performed without tagging. Furthermore, although one can study the azimuthal correlations already from single-tag events, the double-tag mode yields more information. In any case the measurement of the total $\gamma\gamma$ hadronic cross sections can *only* be carried out in the double-tag mode. Finally we note that the tagging will also serve to pre-select the relatively rare $\gamma\gamma$ events from the more abundant annihilation background. Inversely it could also be useful to flag the $\gamma\gamma$ background in the CP violation experiment.

3.2 Tagging at DAΦNE

In order to resolve these questions, we have carried out extensive Monte-Carlo simulations of the process $ee \to ee\pi\pi$. Outgoing generated electrons were tracked from the reaction vertex (taken to be at the intersection point) to various locations along the beam pipe. In all of these calculations the beam energy and the crossing angle of the incident beams were fixed at $E_{beam} = 0.510$ GeV and $\theta_{beam} = 12.5$ mrad at the intersection point. In addition we have assumed a complete compensation for the electrons at the compensator and a magnetic field of 0.6 Tesla in KLOE. The geometry and current settings of the quadrupole, magnets and compensator at the interaction region of DAΦNE is still not finalized but our results refer to the Feb. 1993 version.

In practice, we have calculated the fraction (acceptance) of the final state electrons which are scattered into various regions (Fig. 9), their distribution lateral to the beam axis (z), their ($x-y$ plane) profile and their angular and energy distributions. In Table 5 we list the acceptance for electrons scattered into:

1) the KLOE detector ($\theta > 9.0^o$)
2) the front of the first low β insertion quadrupole ($4.0^o < \theta < 9.0^o$)
3) the region of the end walls ($2.0^o < \theta < 3.0^o$)
4) the regions of coils of the split field magnet (SFM) ($\theta < 2.0^o$)
5) the front of second quadrupole of the triplet downstream the SFM ($\theta < 1.0^o$)

Electrons scattered at angles $\theta > 9.0^o$ have been analyzed with the GEANFI program in order to get the KLOE reconstruction efficiencies.

In Fig. 10 the hit distribution in the central detector tracking chamber is shown. It seems that there is not a great possibility of track reconstruction, owing to the small number of

Table 5: Double and single tagged $e^-e^+ \to e^-e^+\pi\pi$ events (%)

Double Tag	KLOE[2]				
KLOE[2]	0.8	WAT			
WAT	1.4	0.7	Solenoid		
Solenoid	1.1	1.0	0.4	Coils	
Coils	2.3	2.1	1.8	1.8	SAT
SAT	5.8	4.5	5.5	11.3	6.3
Single Tag[1]	17.2	15.2	14.7	27.0	51.7

1) Single tags are summed over the 2 electrons.
2) Requiring at least 6 hits in the KLOE drift chamber these acceptances will be reduced by a factor 6.

hits in the drift chamber. If one require at least 6 hits in the chamber with the impact point on the end-wall calorimeter, the acceptance for these electrons goes down from 17% to 3%. One of this good electron is shown in Fig. 11. Besides from a very preliminary analysis $\simeq$ 90% of the tracks hit the end wall calorimeter.

The electrons scattered in front of the first low β quadrupole cover a very small solid angle, nevertheless their acceptance is reasonable high. A detector covering this region (we refer to this as the wide angle tagger, WAT) has a good reconstruction efficiency ($>$ 90%), because it is orthogonal to the electron direction. We expect that an extended WAT detector covering the full angular region (70$-$300 mrad) should also optimize KLOE electron tracking efficiency, adding at least one space point.

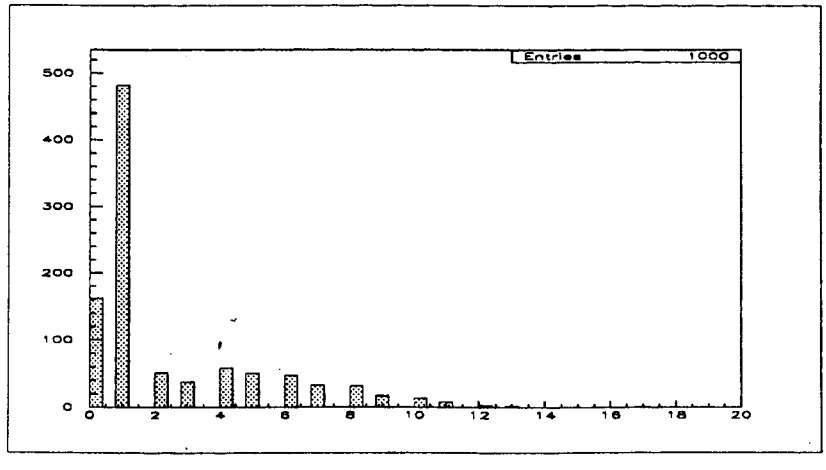

Figure 10: Number of hits into the KLOE drift chamber (normalized to 1000 entries)

Part of the electrons emitted at smaller angles hit the Split Field Magnet (SFM) coils and are lost. The forward tagger should be positioned as near as possible to the beam pipe at a distance from the interaction point that maximizes the acceptance. We have required

Table 6: Double and single tagged $e^-e^+ \rightarrow e^-e^+\pi^0\pi^0$ events/year

Double Tag	KLOE[2]		
KLOE[2]	1	WAT	
WAT	14	43	SAT
SAT	52	280	400
Single Tag[1]	170	940	3200

1) Single tags are summed over the 2 electrons.
2) For KLOE drift chamber we require at least 6 hits.

that these electrons be separated by at least 4 cm from the main beam. Compatible with the machine needs and priorities, we propose to insert the forward tagger at $\simeq$ 8 m from the interaction point. The space now available in this region may allow to detect and identify the scattered electrons. Hereafter we refer to it as the small angle tagger (SAT).

From the results listed in Table 5, one can conclude that the very forward region (SAT) would be most suitable for tagging with an acceptance of about $\simeq$ 50% single-tag mode. The front of the first low beta quadrupole region exhausts $\simeq$ 15% and could be used to insert the wide angle tagger WAT (Fig. 9). There is still a fraction of $\sim$ 15% of the electrons which are scattered to the end walls. This could be in principle exploited should there be enough free space for a tagger.

We can give a first estimate of the expected $\gamma\gamma \rightarrow \pi^0\pi^0$ yield multiplying the electron acceptances given in Table 5 for the $\pi^0\pi^0$ KLOE reconstruction efficiency (87%) and P_T cut (71% if $P_T \leq 45$ MeV/c).

For a luminosity of $L \simeq 5 \times 10^{32}$ cm^{-2} s^{-1} in a year of data taking (10^7 s) the number of fully reconstructed tagged events is given in Table 6.

Hadronic contamination in tagged events

In this paragraph we briefly discuss the contamination coming from the annihilation processes followed by a hadronic tag. A large fraction of these events can be suppressed by the time of flight measurement given by the SAT counters.

In fact for the maximum tagged momentum envisaged for this tagger the arrival time separation between electrons and pions is already about 2 ns taking 8 m to be the distance between the interaction point and the location of the SAT. This time separation is well within the current time measurement resolutions.

Next, let's consider for example the following reaction (see also Table 4) :

$$e^+e^- \rightarrow \phi \rightarrow K^0_S K^0_L \rightarrow \pi^+\pi^- 3\pi^0$$

In this case the annihilation event could provide an hadronic event in KLOE and one (or two) charged particle(s) on the taggers. Detailed Monte-Carlo simulations show that in single tag-mode, 1% of the charged pions hit the WAT and practically none hit the SAT. So the SAT is safe.

For the WAT, it is reasonable to assume 99% probability to detect a π^0 in KLOE, a reconstruction efficiency for charged particles of 95% and a ratio of $\simeq$ 15 between $\gamma\gamma$ and

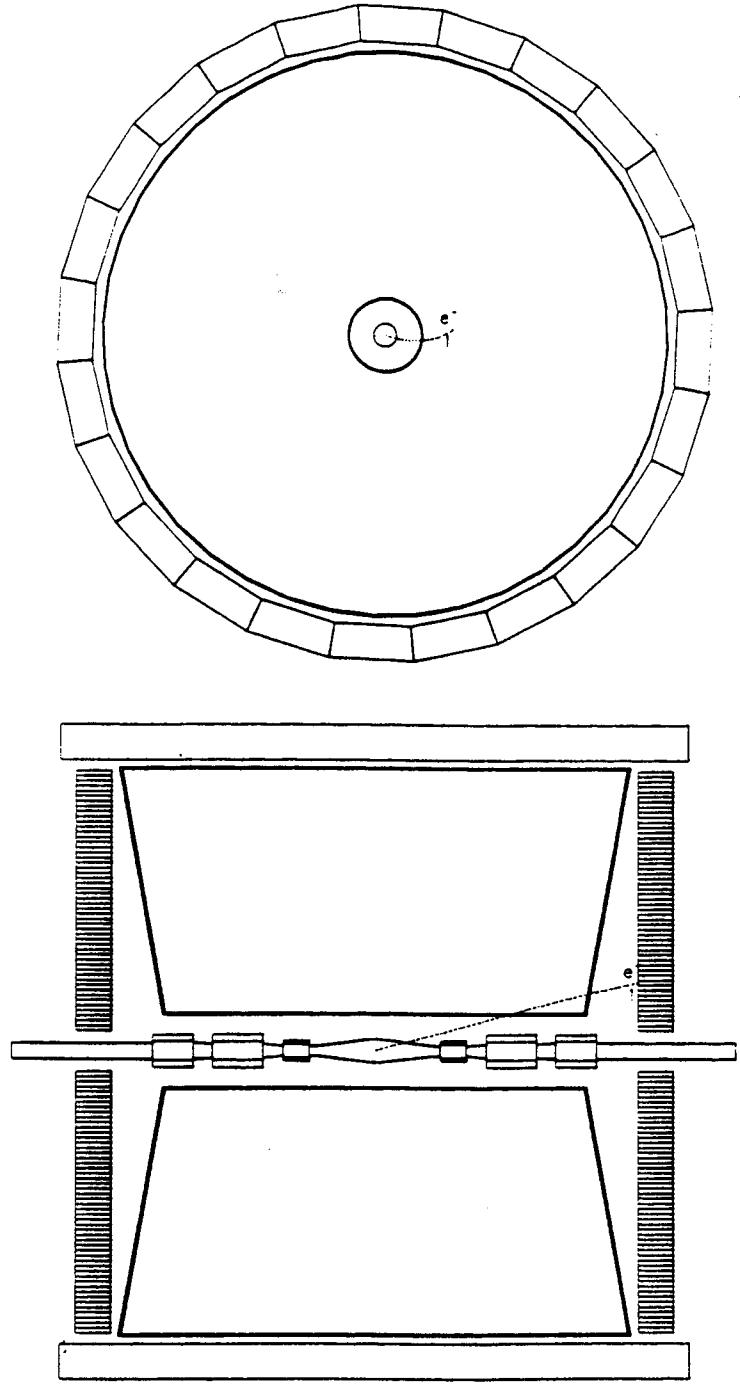

Figure 11: $r-\phi$ projection and top view of one electron with 6 hits in KLOE drift chamber emerging from a $\gamma\gamma$ collision

annihilation acceptances on the WAT. With this assumption we obtain a rejection factor of $\simeq 3 \times 10^4$; if we then add also cuts on $\sum P_T^2$ the total rejection factor is $\simeq 9 \times 10^5$ which should give the possibility to detect the $e^+e^- \to e^+e^-\pi^0\pi^0$ process already in single tagging. We expect the contamination from other sequences of decays such as

$$e^+e^- \to \phi \to K_S^0 K_L^0 \to \pi^0\pi^0\pi^+\pi^-\pi^0$$

to be less important.

3.3 The SAT, WAT and BREM Detectors

The SAT Detector

The SAT detectors will be located downstream of the SFM at $\simeq$ 30 cm from the first quadrupole, on both sides of the interaction region, for tagging of electrons and positrons. It was discussed with the DAΦNE collider crew to enlarge the size of this quadrupole in order for it not to cut the tagged electrons that can be spread to a distance of 30 cm from the primary beam.

The design of the SAT should be tailored according to the features of the electrons to be tagged, the expected background, space and hardware restrictions. Results from Monte-Carlo calculations are shown in Fig. 12 where the SAT should be installed at $\simeq$ 8 m from the interaction region. In the figure we show the radial profile, the energy and angular distributions of the scattered electrons and the corresponding invariant mass $W_{\gamma\gamma}$ range that will be available for our investigations. From these distributions we conclude that the SAT should extend in the horizontal plane of the collider from -4 to $\simeq -30$ cm, measured from the primary beam trajectory (toward the center of DAΦNE). In order to accomplish this request a new design of the quadrupole facing SAT is needed. In Fig. 9 a sketch of this new quadrupole (QSAT) is shown. This quadrupole should have an horizontal aperture of $\simeq$ 30 cm wheras the other dimensions do not have to be changed.

As the tagged electrons emerge at very small angles, we expect at the same angular range a high electron flux from radiative Bhabha ($e^+e^- \to e^+e^-\gamma$) and double radiative Bhabha ($e^+e^- \to e^+e^-\gamma\gamma$) scattering as well as from beam-gas bremsstrahlung. The single gamma radiative Bhabha cross section, integrated over all the SAT acceptance has been evaluated to be $\simeq$ 70 mbarn at most [53]. Assuming the designed single bunch luminosity for DAΦNE of $L_0 = 4.5 \times 10^{30}$ cm^{-2} s^{-1} and the given frequency revolution of 3.17 MHz we expect a rate/bunch of $\simeq$ 0.3 MHz which corresponds to a radiative Bhabha every 10 bunch crossing. Thus the total rate on SAT will be $\simeq$ 40 MHz for 120 circulating bunches. Measurement of the Bhabha photon yield was a routine measurement for many years at Adone [54]. Extrapolating the Adone results to DAΦNE we expect [55] a rate/bunch of $\simeq$ 0.2 MHz which is consistent with the calculated one.

The SAT should perform the following tasks:

a) Record the electrons from $\gamma\gamma$ reactions.
b) Determine the hit position in the x-direction, which in turn measures the electron energy.
c) Identify the nature of the hitting particle, *i.e.*, separate electrons from muons and pions.
d) Eliminate other possible sources of background such as stray electrons.

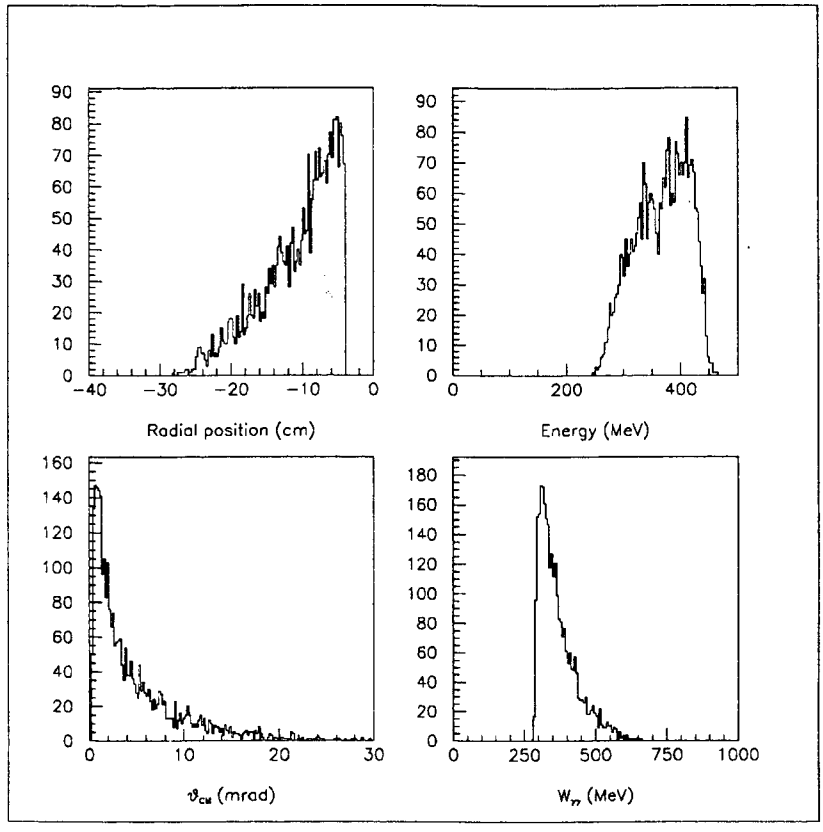

Figure 12: Scattered electron position, energy (MeV) and angular (rad) distributions at the SAT position. The produced $\pi\pi$ mass distribution is also shown.

In Fig. 13 a layout of the proposed SAT is shown. Its physical size is about 30 cm wide $\times$ 7 cm high.

The detector is composed of two hodoscopes separated by 30 cm. Each hodoscope is composed of two parallel planes of scintillating fibers of 1 cm diameter bundles, staggered one with respect to the other by 0.5 cm. These hodoscopes will exploit the maximum energy resolution given by the beam transport optics, and will also serve for a time measurement to be used for e/π separation. The combination of two hodoscopes will give a position (x) and also divergency angle (x') measurement. A large mismatch between position and angle compared to expectation will identify a track as being a background particle. In Fig. 14, the electron energy versus its x position is shown in the upper figure. The lower figure shows the energy resolution as a function of the electron energy expected assuming a 0.5 cm spatial resolution for the SAT hodoscope structure. The hodoscope will be followed during tests by a movable lead scintillating fiber calorimeter of the type described in Refs. [57] and [58], having in total 12 radiation lengths. It will be positioned between the hodoscopes only for tests, not during data taking. It will be built out of two 9.6 cm thick by 3.2 cm wide cells to allow sampling the energy at two intervals along the shower axis, to be able to separate electrons from hadrons. This calorimeter will have an energy resolution of approximately $5\%/\sqrt{E(\mathrm{GeV})}$ [58]. This calorimeter is needed to calibrate and monitor the hodoscopes during set-up at low rates, when DAΦNE operates at low rates or for the low rate region of the hodoscopes. One can then check how the relation between the hit position of the tagged electron and its energy depend on the beam transport optics. It can be used to help understand other monitors of the beam transport optics. One such monitor is the ratio fixed by a measurement of the total flux on the hodoscopes normalized to the KLOE Bhabha

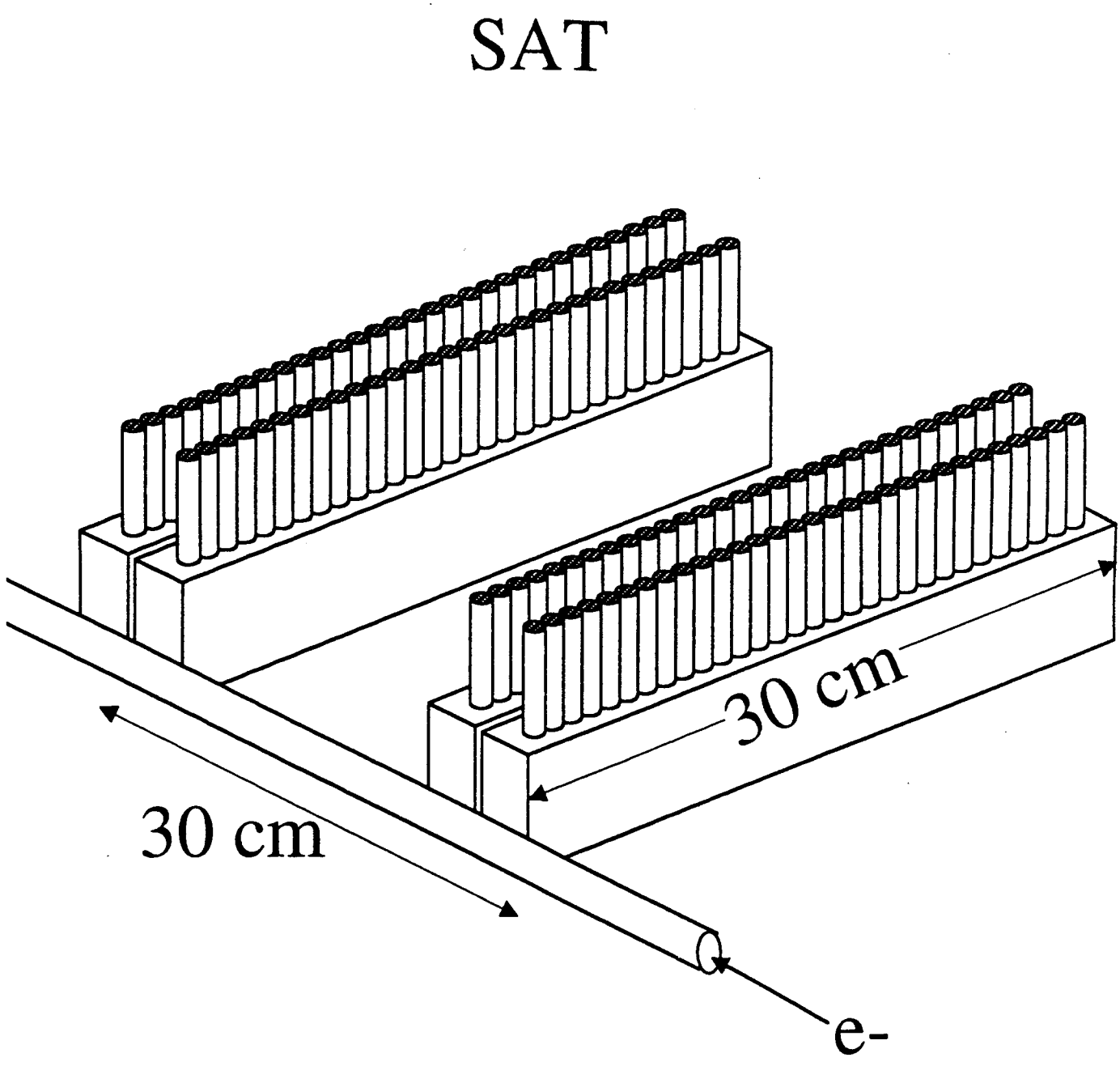

Figure 13: A sketch of the small angle tagger SAT. It is constructed of two hodoscopes 30 *cm* apart. Each hodoscope is composed of two parallel planes of scintillating fibers of 1 *cm* diameter bundles, staggered one with respect to the other by 0.5 *cm*.

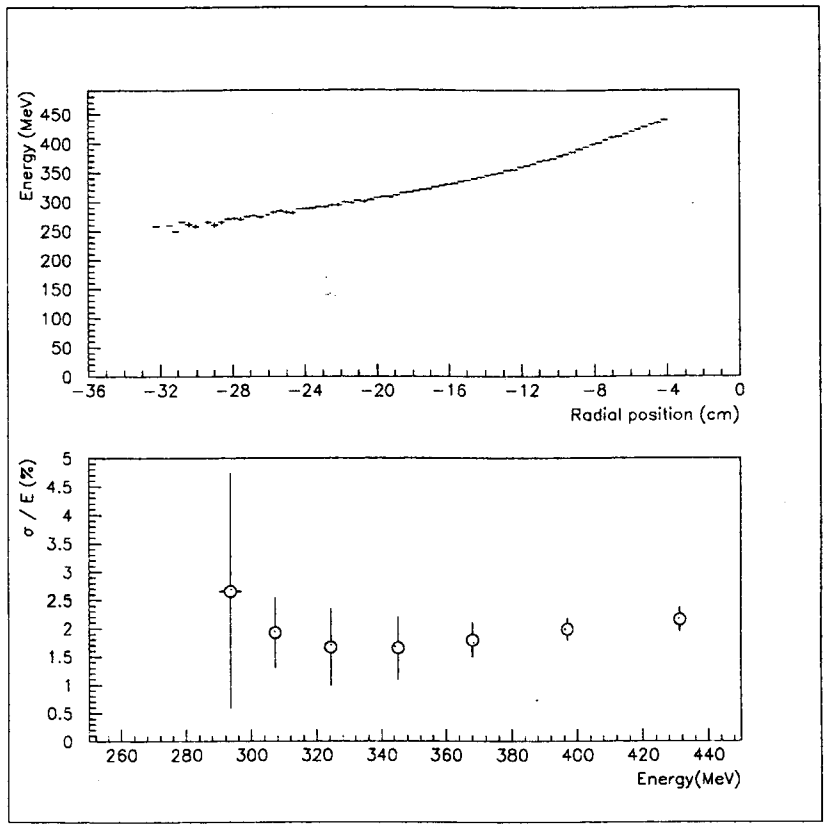

Figure 14: Energy (MeV) position (cm) and energy resolution distributions at the SAT location.

luminosity measurement. The value of this ratio will vary in response to changes in the beam optics. The calorimeter can be used when its rate will not exceed 5 MHz, corresponding to an average of 200 ns between pulses. In that case, the calorimeter adjusted to have a 10-15 ns pulse shape should give a reliable energy measurement and particle identification.

The summary of the possible SAT structure follows:

Hodoscope

cell size 7 cm × 1 cm × 1 cm

cell number 120

Calorimeter

cell size 3.2 cm × 7 cm × 9.6 cm

cell number 2

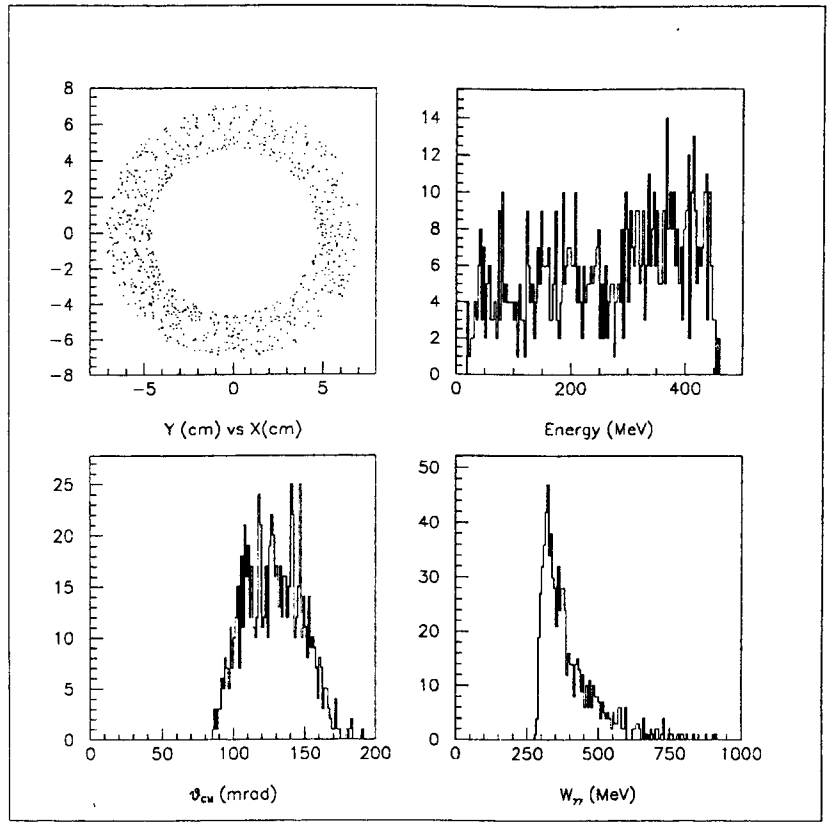

Figure 15: $x-y$ profile, energy (MeV) and angular (rad) distributions at the WAT position. The produced $\pi\pi$ mass distribution is also shown.

The WAT Detector

Fig. 15 shows the $x-y$ profile, the energy, angular and hadronic mass distributions for electrons measured at $\simeq$ 45 cm from the interaction region. This region is free from radiative Bhabha events, but the hadron contamination from annihilation events is of the order of 1%.

Because the detector is located very near to the interaction region, there is only space for a tracking device, with no calorimeter. A possible solution could be the use of silicon detectors placed around the beam pipe, covering the polar angle between 4^o and 9^o.

The BREM Detector

The BREM (bremsstrahlung) detector is intended to detect the γ's produced in the radiative Bhabha process in order to increase the SAT rejection background power. The cross section of proces $e \rightarrow e\gamma$ is $\simeq$ 130 mbarn [53] for γ's with energies larger than 20 MeV that corresponds to a total rate of $\simeq$ 65 MHz. With such a high rate also a lead-scintillating fiber calorimeter of the type described in Refs. [57] and [58] has problems of pile-ups. We are studying the possibility to use a $\hat{C}$erenkov material like the PbF_2 electromagnetic calorimeter recently proposed for RHIC [59]. Lead Fluoride is a $\hat{C}$erenkov material with very high density (7.77 g cm^{-3}), a short radiation length (9.3 mm) and a small Moliére radius (2.2 cm). It does not produce as much light as scintillating crystals but is much faster

and its light output is equal or better than lead glass with a good optical transmission extending down below 300 nm. A prototype has been built and tested at the Brookhaven AGS [60]. The results obtained show an energy resolution in the energy range $1 - 4$ GeV of $\simeq 5.1\%/\sqrt{E(\mathrm{GeV})}$, a yield bigger than 1.3 photoelectron/MeV and useful signals down to 32 MeV.

The detector has shown a rather good radiation hardness up to $\simeq$ 30 Krad with a more severe damage up to $\simeq$ 1.0 Mrad. These results show a big improvement over the initial samples which were measured in 1990 [61]. This is mainly due to improvements in the purity of the raw material and in the growth and processing techniques used to produce the crystals. It is likely that the radiation hardness could be increased even further with further study.

4 Luminosity

The physics goals outlined in this proposal require absolute measurements of cross sections. Hence, there is a need for a precise measurement of the differential and integrated Luminosity of DAΦNE during data taking. One can rely on the measurement of two pure QED processes, the Bhabha scattering and the radiative Bhabha scattering. We estimate [62] that at $\sqrt{s} = 1$ GeV and already for the designed Luminosity at the starting time of DAΦNE of $L \simeq 10^{32}$ cm^{-2} s^{-1}, the rate of Bhabha scattering entering KLOE (9^o to 171^o) is of the order of 4.5 kHz. At the same luminosity the rate of the radiative Bhabha electrons measured by SAT is of the order of few MHz.
This luminosity measurament can be cross-checked against the pure QED $\gamma\gamma \to \mu^+\mu^-$ process, which also can be measured; $\gamma\gamma \to \mu^+\mu^-$ cancels most of the systematic errors of the process $\gamma\gamma \to \pi^+\pi^-$.

5 Conclusions

We have shown the feasibility to carry out high precision measurements of two-photon reactions leading to low mass hadron(s) with the KLOE detector designed for DAΦNE.
This measurements can be performed by equipping the detector with the electron tagging facilities, described in this report, that we summarize for convenience:

a) Two forward (SAT) detectors.
b) Two bremsstrahlung (BREM) detectors. The installation of these detectors requires a new design of the pipe, downstream of the split field magnet until the quadrupole that faces SAT. This quadrupole (QSAT shown in Fig. 9) should be redesigned, having an horizontal aperture of $\simeq$ 30 cm.
c) Two wide angle (WAT) detectors.

The two-photon physics topics which can be covered in that experimental set-up, are:

(1) Precision measurements of the polarizabilities of charged and neutral pions via the two photon reactions of the type $\gamma\gamma \to \pi\pi$. These will allow to test chiral theories and chiral perturbation techniques.

(2) One will be able to measure for the first time the azimuthal correlations of the $\gamma\gamma \to \pi\pi$ reaction. We expect in this case to identify $\pi\pi$ events with a adequate efficiency to allow very clean and precise measurements for testing various models of hadronic production near threshold.

(3) Formation of the $C = +1$ light pseudoscalar mesons, π^0, η and η' can be investigated with a high precision and will allow the study of the $q\bar{q}$ and possibly gg inner structure. For the π^0 its measured radiative width will also improve the currently known life-time.

(4) The possibility to realize a double tagging at DAΦNE will allow reliable measurements of the total $\gamma\gamma \rightarrow$ *hadrons* cross section below 1 GeV, which currently is vaguely known, to be compared with several models.

6 Acknowledgements

We would like to thank G. Vignola for his co-operation in the possible adaptation of DAΦNE to the tagging needs. We gratefully acknowledge the help of P. Franzini and the KLOE collaboration, in supplying us with detailed information on the design and performance of the detector and for letting us use their Monte-Carlo program. Thanks are also due to M. Greco and O. Nicrosini for the big effort put in the study of radiative Bhabha at very small angle. Finally we would like to thank G. Bencivenni and G. Felici for suggestions on the technique to be used for the WAT detector.

References

[1] "KLOE, A General purpose detector for DAΦNE", LNF-92/019(R).

[2] A. Courau, in " DAΦNE, The Frascati ϕ Factory ", (G. Pancheri, Ed.), (1991) 373.

[3] V.A. Petrun'kin, Sov. J. Part. Nucl. 12 (1981) 278.

[4] S. Bellucci and D. Babusci, Proceedings of the Frascati Workshop for Detectors and Physics at DAΦNE, Frascati,Italy, April 9-12, (1991) 351.

[5] A. Courau and G. Pancheri, in "The DAΦNE Physics Handbook", (L. Maiani, G. Pancheri and N. Paver, Eds.), (1992) 353.

[6] V.A. Petrun'kin, Sov. J. Part. Nucl. 12 (1981) 278.

[7] B.R. Holstein, Comments Nucl. Part. Phys. 19 (1990) 239.

[8] M.A. Moinester, Proceedings of the Conference on the Intersections Between Particle and Nuclear Physics, Tucson, Arizona, 1991, AIP Conference Proceedings 243, P553, 1992, Ed. W. Van Oers.

[9] D. Babusci, S. Bellucci, G. Giordano and G. Matone, Frascati Preprint, LNF-92/071 (1992), to appeare in Phys. Lett. B (1993),
D. Babusci, S. Bellucci, G. Giordano and G. Matone, Proceedings of the Workshop on Hadron Structure from Photo-reactions at Intermediate Energies, Brookhaven National Laboratory, May 1992, (A.M. Nathan and A.M. Sandorfi, Eds.), BNL Report BNL 47972.

[10] V. Bernard, B. Hiller and W. Weise, Phys. Lett. B159 (1988) 85.

[11] V. Bernard and D. Vautherin, Phys. Rev. D40 (1989) 1615.

[12] M.A. Ivanov and T. Mizutani, Phys. Rev. D45 (1992) 1580.

[13] D. Babusci, S. Bellucci, G. Giordano, G. Matone, A. M. Sandorfi and M.A. Moinester, Phys. Lett. B277 (1992) 158.

[14] J. Gasser and H. Leutwyler, Ann. of Phys. 158 (1984) 142.

[15] J. Bijnens and F. Cornet, Nucl. Phys. B296 (1988) 557.

[16] J.F. Donoghue, B.R. Holstein and Y.C. Lin, Phys. Rev. D37 (1988) 2423.

[17] J. Gasser and H. Leutwyler, Nucl. Phys. B250 (1985) 465; J.F. Donoghue and B.R. Holstein, Phys. Rev. D40 (1989) 2378.

[18] P. Ko, Phys. Rev. D41 (1990) 1531,
J. Bijnens, S. Dawson and G. Valencia, Phys. Rev. D44 (1991) 3555.

[19] J. F. Donoghue, C. Ramirez and G. Valencia, Phys. Rev. D39 (1989) 1947.

[20] Particle Data Group, Phys. Rev. D45 part II (1992) 1.

[21] S. Bellucci, in "The DAΦNE Physics Handbook", (L. Maiani, G. Pancheri and N. Paver, Eds.), (1992) 419.

[22] MARK-II Coll. (J.Boyer et al.), Phys. Rev. D42 (1990) 1350.

[23] Yu.M. Antipov at al., Phys. Lett., 121B (1983) 445,
Yu.M. Antipov at al., Z. Phys., C26 (1985) 495.

[24] PLUTO Coll. (Ch. Berger et al.), Z. Phys. C26, (1984) 199.

[25] A. Courau et al., Phys. Lett. 96B (1980) 402; Nucl. Phys., D271 (1986) 1.

[26] Z. Ajaltouni et al.,Phys. Lett. 194B (1987) 573.

[27] T.A. Aibergenov et al., Czech. J. Phys., B36 (1986) 948.

[28] Crystal Ball Coll. (H. Marsiskie et al.), Phys. Rev. D14 (1990) 3324.

[29] M.R. Pennington, in "The DAΦNE Physics Handbook", (L. Maiani, G. Pancheri, N. Paver, Eds.), (1992) 379.

[30] S. Bellucci, J.Gasser and M. Sainio, invited talk given by J. Gasser at the Eurodaφne Workshop, April 19-23, 1993, Frascati.

[31] J.F.Donoghue and B.R.Holstein, UMHEP-383 (1993).

[32] S. Bellucci and G. Colangelo, Frascati Preprint, LNF-93/013 (P).

[33] D. Babusci, S. Bellucci, G. Giordano, G. Matone and M. Candusso, INFN Report KLOE-92/22.

[34] A. Courau, Proceedings of the Frascati Workshop for Detectors and Physics at DAΦNE, Frascati, Italy, April 9-12, (1991) 373.

[35] S. Ong and P. Kessler, Mod. Phys. Lett. A Vol. 2 No. 9 (1987) 683; S. Ong, P. Kessler and A. Courau, Mod. Phys. Lett. A Vol. 4 No. 10 (1989) 909.

[36] S. Ong, "Test of Chiral Loops and Azimuthal Correlations in the Reaction $\gamma\gamma \to \pi^0\pi^0$", Preprint LPC 9301 (1993), Laboratoire de Physique Corpusculaire, College de France, Paris, France.

[37] CELLO Coll. (H.J. Behrend et al.), Z. Phys. C49, (1991) 401.

[38] Crystal Ball Coll. (D.A. Williams et al.), Phys. Rev. D38 (1988) 1365.

[39] Ll. Ametller, J. Bijnens, A. Bramon and F. Cornet, Phys. Review D45, (1992) 986.
J. Bijnens, A. Bramon and F. Cornet, Phys. Rev. Lett. 61, (1988) 1453.

[40] The $BR(f_0(975) \to K\overline{K})$ derivation and its value has recently been questioned, see e.g., G. Alexander,LNF-93/001(P).

[41] A. Backer, "Unfolding Techniques" in Proc. of the VIth Int. Workshop on Photon-Photon Collisions, (R.L. Lander, Ed.), Lake Tahoe, California, September 10-13, 1984, p. 205.

[42] PLUTO Coll. (Ch. Berger et al.), Phys. Lett. 149B (1984) 421.

[43] TPC/2γ Coll. (D. Bintinger et al.), Phys. Rev. Lett. 54 (1985) 763.

[44] See e.g., G. Alexander, "The $\gamma\gamma$ Total Cross Section and the Photon Structure Function", Proc. VIIth Int. Workshop on Photon-Photon Collisions (A. Courau and P. Kessler, Eds.), Paris, April 1986.

[45] G. Alexander and U. Maor, Phys. Rev. D46 (1992) 2882.

[46] G. Alexander, U. Maor and C. Milstene, Phys. Lett. 131B (1983) 224.

[47] G. Alexander, A. Levy and U. Maor, Z. Physik C30 (1986) 65.

[48] A. Levy, Phys. Lett. B177 (1986) 106; ibid. B181 (1986) 401.

[49] G. Ecker, in "Hadronic Matrix Elements and Weak Decays", Proc. of the Workshop (A.J. Buras et al., Eds.), Ringberg Castle, Germany, 1988.

[50] Ll. Ametller, J. Bijnens, A. Bramon and F. Cornet, Phys. Lett. B276, (1992) 185.

[51] P.Ko, Phys. Rev. D47, (1993) 3933.

[52] F. Anulli et al., in "The DAΦNE Physics Handbook", (L. Maiani, G. Pancheri and N. Paver, Eds.), (1992) 435.

[53] V.N. Baier et al., Physics Reports 78 (1981) 293,
G. Pancheri, "Estimate of small angle radiative Bhabha scattering at DAΦNE", LNF-93/024(P).

[54] H.C. Dehne, M. Preger, S. Tazzari and G. Vignola, "Luminosity measurement at ADONE by single and double bremsstrahlung", Nucl. Instr. and Methods 116 (1974) 345.

[55] M. Preger, A. Antonelli et al., Phys. Lett. B301 (1993) 317.

[56] M. Greco, Private Communication.

[57] S. Bianco et al., "Lead-Scintillating Fibers Calorimetry for Low Energy Photons", presented by S. Sarwar at the it 3rd Int. Conf. on Calorimetry in High Energy Physics, Sept. 29-October 2, (1992), Corpus Christi, Texas,USA.

[58] D. Babusci et al., "Lead-Scintillating Fiber Electromagnetic Calorimeters with $4.8\%/\sqrt{E(\mathrm{GeV})}$ energy resolution in the $20-80$ MeV range", Nucl. Ins. and Methods, A332 (1993) 444.

[59] "Proposal to study Lead Fluoride as a potential High Resolution Electromagnetic Calorimeter for RHIC", BNL-Oak Ridge, October 1991.

[60] "A study on the use of Lead Fluoride for Electromagnetic Calorimetry", Presented at IEEE Nucl. Sci. Symp., Orlando, FL, October 27-31, 1992.

[61] D.F.Anderson et al., Nucl. Instr. and Methods A290 (1990) 385.

[62] G. Colangelo, S. Dubnička and M. Greco, "Radiative Corrections at DAΦNE", in "The DAΦNE Physics Handbook", (L. Maiani, G. Pancheri and N. Paver, Eds.), (1992) 327.